Numerical Pattern of 3D Tornado Rise with Account for Mirror Asymmetry

Alexander Yu. Gubar* and Victor N. Nikolaevskiy

Institute of Physics of the Earth, Russian Academy of Sciences, 10-1, Bol. Gruzinskaya Ul., Moscow, 123995, Russia

Abstract: Authors are returning to the basic concepts of turbulence – homogeneity and symmetry principles. It is shown that the homogeneity in the sense of constant mean velocity gradient (instead of constant velocity) permits to introduce mirror asymmetry. This way is corresponding to stratified atmosphere and to differential volume in any continuum model. The basic ideas of A. N. Kolmogorov do not contradict to such an approach. Moreover, the use of the intrinsic eddy angular velocity (so-called spin or mesovorticity) as the internal thermodynamic parameter becomes necessary for adequate description of tornado (and intensive atmospheric vortices, in general) dynamics. The continuum description is formulated with standard introducing of stresses averaged over a cross-section, and now motivated asymmetry leads to the vortices moment of momentum balance. The set of nonlinear 3D partial differential equations is suggested for the problem of tornado generation from a cloud of initial vortices. The dependence of turbulent rotation viscosity on the spin permits to localize the tornado body due to the nonlinear diffusion effect. Numerical calculations are performed at two different clusters using Parjava program environment. The growth of typical tornado structure is shown by a sequence of pictures. A visual comparison with the Hurricane Isabel, 2003, is represented.

Keywords: Tornado, Vortices, Turbulence, Angular momentum, Mirror Asymmetry, Scaling, Mesovortex.

1. INTRODUCTION

A.N. Kolmogorov [1] made important contributions to the Taylor turbulence theory [2]. He suggested:

(1) To *avoid the isotropy* of the velocity pulsations fields but to save it for the pulsation differences. His *local* isotropy was a great step towards the other cases of mean velocity fields besides the constant velocity (in 1941).

(2) To consider the *energy flux* as the main parameter of energy cascades in turbulence (in 1941). It coincided with the Schrödinger [3] principle for thermodynamically open systems.

(3) To introduce the *rotation frequency* as an additional kinematical parameter (in 1942). Actually, the angular velocity vector was needed, as in the Cosserat continuum [4], but then it is also necessary to overcome the mirror symmetry limitation.

In fact, mirror symmetry is inadequate for a general turbulent flow if the gradient of the mean velocity does exist. This happens in actual profiles of the atmosphere, that were an object of own Kolmogorov research, as well as in the representative turbulent continuum cell, for which the balances of mass, momentum and angular momentum have to be formulated.

Here we use all these suggestions for the development of turbulence theory effective enough for tornado generation.

Mathematically, the mirror asymmetry reveals itself in rising of anti-symmetrical terms in turbulent stress tensor. Along with Cosserat brothers [4], the turbulent theories dealing with this asymmetry were developed by Nikolaevskiy [5-6], Mattioli [7], Ferrari [8], Heinloo [9], Eringen and Chang [10], though probably only Nikolaevskiy and Heinloo (with their co-authors) have applied their theories to geophysical phenomena. First attempt of using asymmetrical turbulent stress tensors in the problem of tornado (and hurricane) bulk modeling was made by Arsenyev, Gubar, Nikolaevskiy [11] (2004) and developed in [12-16]. In this paper we apply the results of 3D tornado speculations in the mirror asymmetry turbulent model to first show in detail how a tornado suction spots [17-23] -- smaller whirls rotating around the main one in the tornado “eyewall” -- can be formed while it rising. Then, using a simple rescaling, we provide a visual comparison of the model tornado suction spots with the “pin-wheel” structure of Hurricane Isabel, 2003, [24-25] and give a quantitative explanation of this phenomenon, alternative to that furnished in [26], where 2D barotropic flow model was used. Although the multiple-vortex structure both in hurricanes and tornados has been numerically modeled earlier (for hurricane-like vortices, egg. in [26]), the mirror asymmetry turbulence theory

*Address correspondence to this author at the Institute of Physics of the Earth, Russian Academy of Sciences, 10-1, Bol. Gruzinskaya Ul., Moscow, 123995, Russia; Tel: +7(925)3143318;
E-mail: parkag@yandex.ru

E-ISSN: 2409-5710/14

presented here is able to provide numerical description of the multiple-vortices formation processes in the both scales.

We introduce the moment of inertia in the evident form that permits us to consider mass components involved in the tornado evolution.

2. NOTE ON THE STRESS TENSOR SYMMETRY

In all approaches to turbulence the Navier – Stokes equations are assumed to be valid for micro flows at a given time moment. In an attempt to develop balance equations, valid at a macro level, we consider a spatial continuum cell bigger than the size of vortices that contains the main turbulent energy (Figure **1**).

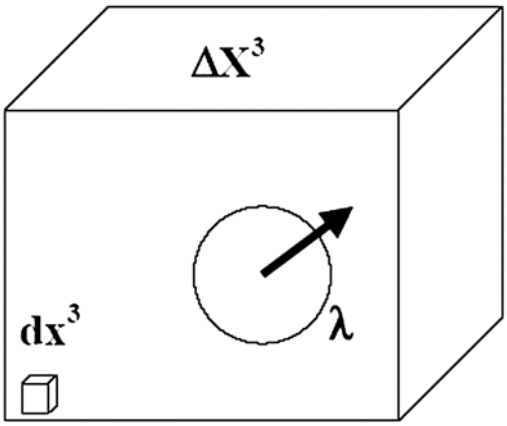

Figure 1: The scales of microelements (dx), macroelements (dX) and mesovortices (λ).

Practically, there are two different scales for an effective turbulent field description. First, there is an element of a turbulent vortex with the volume scale dx^3 that needs in the balances of mass and momentum only, as in the Navier – Stokes equations, because the element's own rotation is negligible due to its small size. This point of view is proved by the inertia moment I estimation: $(I/dx^3) \sim dx^2 << \lambda^2$.

Second, there is a volume scale ΔX^3 including at least one vortex with λ as a radius. Because the vortex, corresponding to the main turbulent energy, possesses sufficiently high angular momentum, its inertia momentum cannot be missed in the balance equation for the angular momentum and its special evolution has to be developed.

However, the volume, which size is selected (by the macro continuum nomination) to be much less than the outside problem scale, has to include the gradients of macrovariables beginning with mean velocity ***U*** up to mean stresses, all of which appear in the macro balance equations and in the interconnecting governing "laws".

Therefore, the adequate statistical image should be homogeneous relatively to *gradients* of the mean variables, and the random field w_i under consideration depends at least on one vector. Because the distance ***r*** between two points is a vector, the corresponding correlation tensor $C_{ij} = \langle w_i(\boldsymbol{X})\, w_j(\boldsymbol{X}+\boldsymbol{r})\rangle$, $u_i = U_i + w_i$ is not symmetrical but a function of the angle between ***r*** and **grad *U*** (Figure **2**). This point was first mentioned in [5] and corresponds to the case of *gradient homogeneity*.

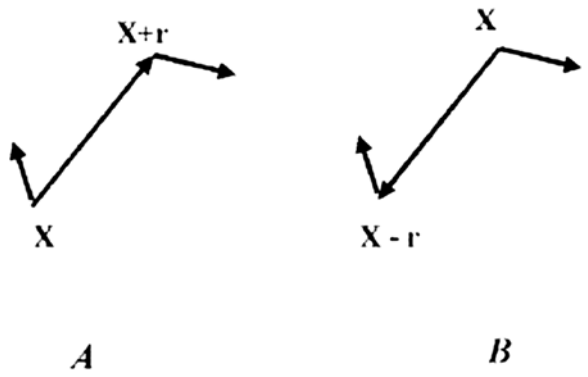

Figure 2: Illustration to possibility of asymmetry of the correlation (as well as the stress) tensors.

Consequently, the mirror reflection does change the results of statistical averaging in the homogeneity case determined as velocity gradient constancy. Therefore, the introduction of the angular velocity **ω** (and pseudovectors in general) as a kinematic variable is quite adequate in the turbulence theory.

The Reynolds stress tensor $R_{ij} = -\langle \rho w_i w_j \rangle_j$ has to be introduced only by the Cauchy method as a momentum vector ρw_i transferred with the velocity pulsation w_j across the plane oriented by its normal $n_j = w_j/|w_j|$. Here ρ is the density and $\langle\ \rangle_j$ is a symbol of averaging at a cross-section ΔX^2 with the normal n_j.

The tensor ρC_{ij} at $r \to 0$ may be identified with the same momentum flux through the differential plane element dx^2, averaged statistically. The results of these two averaging should coincide, if the ensembles of dx^2 statistics and over the plane ΔX^2 are equivalent.

Besides, the limiting process $r \to 0$ does not exclude the dependence of ρC_{ij} on **ω** because "zero" is here understood as relatively to the macroscale**.** This means that the stress tensor in both cases is asymmetric potentially.

3. AVERAGED EQUATIONS

The deriving of effective balance equations for differential cells, which size is bigger than the turbulent eddies scale λ, means the spatial averaging [5,6] of the Navier – Stokes equations valid for the scale d*x* less than λ:

$$\begin{aligned}
&\partial_t <\rho> + \partial_j <\rho u_j> = 0,\\
&\partial_t <\rho u_i> + \partial_j <\rho u_i u_j>_j = \partial_j <t_{ij}>_j + <f_i>,\\
&\partial_t <\varepsilon_{ilk}\rho\xi_l u_k> + \partial_j <\varepsilon_{ilk}\rho\xi_l u_k u_j>_j\\
&\qquad = \partial_j <\varepsilon_{ilk}\xi_l t_{kj}>_j + <\varepsilon_{ilk}\xi_l f_k>,
\end{aligned} \tag{1}$$

where all the functions are stochastic in space, t_{ij} is the stress tensor assumed to be symmetric in the scale d*x*, f_i are the external forces, ε_{ijk} is the alternating Levi – Civita tensor, $\xi_i = x_i - X_i$, $<\rho\xi_i> = 0$. The resulting equations for the mean fields of the velocity U_i, angular momentum M_i, and pressure P include[1] the Reynolds stresses R_{ij}:

$$\begin{aligned}
&\partial_t\rho + \partial_j\rho U_j = 0, \quad \rho D_t U_i = \partial_j(R_{ij} - \delta_{ij}P) + f_i,\\
&\rho D_t M_i = \partial_j\mu_{ij} + \varepsilon_{ijk}R_{kj} + G_i, \quad D_t = \partial_t + U_j\partial_j,
\end{aligned} \tag{2}$$

where μ_{ij} is the Mindlin couple stresses also acting at the cell faces, $M_i = J_{ij}F_j$, J_{ij} is the vortex moment of inertia[2], and, $\boldsymbol{F}=\boldsymbol{\Omega}+\boldsymbol{\omega}$, $\boldsymbol{\Omega}=0.5$ **rot** $\boldsymbol{U}$, $\omega_i=0.5\varepsilon_{ijk}<\partial w_k/\partial\xi_j>$ are the total, macro- and meso- vorticities, respectively[3]; $\boldsymbol{f}$ and $\boldsymbol{G}$ are the averaged external forces and momenta. The traditional turbulence governing laws now connects the asymmetric part of the Reynolds stresses with spin rotation of a vortex and the couple stresses with the angular momentum gradient**:**

$$\begin{aligned}
&0.5\left(R_{ij} + R_{ji}\right) = \rho K_1 2e_{ij},\\
&0.5\left(R_{ij} - R_{ji}\right) = \rho K_2\varepsilon_{ijk}\omega_k,\\
&m_{ij} = \rho K_3\partial_j M_i,
\end{aligned} \tag{3}$$

where $e_{ij} = 0.5\,(\partial_i U_j + \partial_i U_j)$ is the strain rate. For the evolution of the specific moment of inertia $J_{ij} = (\delta_{ij}\delta_{kl} - \delta_{ik}\delta_{jl})<\rho\xi_k\xi_l>/\rho$ derived in [5] we use the simplified form:

$$\rho D_t J = \partial_j\left(\rho K_3\partial_j J\right), \tag{4}$$

where J is assumed to have spherical symmetry: $J_{ij}=\delta_{ij}J$.

The total (molecular + turbulent) kinematic viscosity coefficients $K_1,\ldots K_3$ have to correspond to the internal energy flux principle, that is, they depend on the dissipation function of turbulent field. This means that the rheological links for turbulence flows are essentially nonlinear. The latter is in accordance with observed localization of turbulent objects, for example, tornado in the surrounding atmosphere. This is analogous to the "fire ball" in the atmosphere generated by atomic explosion explained by nonlinear temperature dependence of thermal conduction in gases [29].

The averaged equations (2)-(4) should be completed with the thermodynamic relations: the total energy conservation law and the gas state equation. For the adiabatic processes, (2)-(4) lead to the following total energy E evolution equation

$$\partial_t E = \partial_j P_j - E_{dis} + W \tag{5}$$

where $E = \rho(E_{macro} + E_{meso} + E_{in})$, $E_{macro} = 0.5U^2$, $E_{meso} = 0.5JF^2$ are the specific macro, meso, and inner energy, respectively, $P_j = U_i(R_{ij} - \delta_{ij}(P+E)) + \rho K_3\partial_j E_{meso}$ is the total energy flux per volume unit, W is the power of the external forces and momenta, $E_{dis} = \rho(2K_1 e_{ij}e_{ij} + 2K_2\omega_s\omega_s + JK_3(\partial_i F_j)^2)$ is the total energy dissipation rate, which is always positive, and, therefore, K_1, K_2, $K_3 > 0$. The coefficients K_k have been discussed in [12-13]: $K_k = \nu_k + K_{Tk}\,(J\omega\ldots)$, where $k = 1,\ldots3$, ν_k and K_{Tk} are the kinematical molecular and turbulent viscosity coefficients, respectively, and $K_{Tk} >> \nu_k$. The turbulent viscosity coefficients K_{Tk} have the form [12]

$$K_{T1,3} = C_1 J\omega, \quad K_{T2} = \alpha_2 K_{T1} \tag{6}$$

where $\alpha_2 \sim (\Lambda_1/\Lambda)^p << 1$, $p>0$, Λ_1 is the sub-meso scale: $\lambda_0 << \Lambda_1 << \lambda \le \Lambda << L$, $\lambda_0 \sim (\nu_1^3/\varepsilon)^{1/4}$ is the inner scale of turbulence, ε is the turbulent energy dissipation rate [30], $\Lambda \sim J^{1/2}$ and L are the meso and macro scale, respectively. The model coefficient C_1 in (6) corresponds to the model coefficient C in the paper [31], where a different meso scale turbulent model is studied. In [12] we evaluated the turbulent dissipation rate ε as the dissipation at the Λ-scale, which according to (5)-(6) can be estimated as follows: $\varepsilon = E_{dis}^{(\Lambda)} \sim K_{T2}\omega^2 \sim J\omega^3$, and, therefore, the expression (6) agrees with the Kolmogorov – Obukhov concept [30]: $K_T^{(\Lambda)} \sim (E_{dis}^{(\Lambda)}\Lambda^4)^{1/3} \sim J\omega$.

[1]The third equation in its continuum form of angular momentum balance was first introduced by Cosserat brothers [4]. *De facto* its application to the turbulence was suggested by G. Mattioli [7] but the own (spin) rotation of the vortex was introduced much later by C. Ferrari [8].

[2]The vortex inertia tensor was first discussed by H. Poincare [27] and afterwards - by G. Batchelor [28], and Eringen and Chang [10].

[3]Here and then ρ means <ρ> when outside the averaging brackets <>.

In fact, the atmosphere has so-called "background" mesovorticity ω_{bk} and mesoscale $\Lambda_{bk} \sim J_{bk}^{1/2} << \Lambda$ corresponding to the mean coefficient of turbulent mixing for the given scale L [32]. Finally, using the typical constant value of the specific moment of inertia in (6), the total mixing coefficients are given by [11-14]:

$$K_{1,3} = K = A\, f(\omega),\ K_2 = \alpha_2 K, \tag{7}$$

where A is the initial total viscosity coefficient, $f(\omega) = (\omega + \omega_{bk})/(\omega_0 + \omega_{bk})$, $\omega_0 = \|\omega(X, 0)\|_C$.

4. INITIAL BOUNDARY PROBLEM AND NUMERICAL SCHEME

Under our assumptions, the thermodynamic parameters for a two-atomic perfect gas (the air) are interconnected by the adiabatic equation: $\ln(\rho/\rho_0) = 5/2\ \ln(T/T_0) = 5/7\ \ln(P/P_0)$. The initial temperature profile is dry-adiabatic: $T(\boldsymbol{X},0) = T_0\,(1 - \gamma_a z)$, where subscript "0" corresponds to the values at the ground level, T_0 $\gamma_a = g/C_p \approx 0.0098$ K m^{-1} is the dry-adiabatic temperature gradient, $C_p \approx 1005$ J kg^{-1} K^{-1} is the specific air heat at constant pressure, $g \approx 9.8$ m s^{-2} is the acceleration of gravity.

Using a new variable $a(\boldsymbol{X},t) = \ln(\rho(\boldsymbol{X},t)/\ \rho(\boldsymbol{X},0))$, the averaged equations (2)-(4) with the coefficients (7) in the dry-adiabatic compressible rotating atmosphere can be written in the explicit form:

$$\partial_t a = -D_j[U_j],\quad \partial_t J = -U_j \partial_j J + K\Delta J + \kappa_j \partial_j J,$$

$$\begin{aligned}\partial_t U_i = &-U_j\,\partial_j U_i + 2\left(K\,\partial_j e_{ij} + \kappa_j e_{ij}\right) + \varepsilon_{ijk}(\alpha_2 D_j[K\omega_k] + \\ &+ 2U_j\Theta_k) + \delta_{i3} g\left(e^{0.4a} - 1\right) - c^2\,\partial_i a,\end{aligned} \tag{8}$$

$$\begin{aligned}\partial_t F_i = &-U_j \partial_j F_i + K\Delta F_i + \kappa_j \partial_j F_i + \\ &+ \left(2K/J\right)((\partial_j J)\partial_j F_i - \alpha_2 \omega_i) + \varepsilon_{ijk} F_j \Theta_k,\end{aligned}$$

where $D_j[*] \equiv \partial_j * + *\cdot(\partial_j a - \delta_{i3} 2.5\gamma_a/(1 - \gamma_a z))$, $\kappa_j = D_j[K]$, $c^2 = c_0^2 e^{0.4a}\ (1 - \gamma_a z)$ is the square of the speed of sound, $c_0^2 = 7/5\ R_a T_0$ is its value at the ground level, $R_a \approx 287.04$ J kg^{-1} K^{-1} is the dry air specific gas constant, $\boldsymbol{\Theta} = \Theta_0\{-\cos\varphi_0,\ 0,\ \sin\varphi_0\}$, $\Theta_0 \approx 7.29\ 10^{-5}$ s^{-1} is the angular frequency of the Earth rotation, φ_0 is the latitude. The axes $\boldsymbol{X} = \{x,y,z\} = \{x_1,x_2,x_3\}$ are directed to the south, east, and zenith, respectively.

The boundary conditions in the domain $D = \{|x|,|y| < L_1,\ 0 < z < H\}$ are given by

$$\begin{aligned}
&z = 0: && U_{x,y,z} = w_z = 0,\ J = J_{bk},\\
&&& -R_{kz} = \rho C_f\,|V|V_k,\ \left(k = x,y\right),\\
&z = H: && U_z = \partial_z U_{x,y} = \omega_{x,y} = \partial_z F_z = \partial_z J = 0,\\
&|x|,|y| = L_1: && \partial_n U_i = \partial_n F_i = 0,\ \left(i = x,y,z\right),\ J = J_{bk},
\end{aligned} \tag{9}$$

where U_n is the normal derivative at the corresponding boundary, $V_k = V_k(x,y)$ is U_k averaged by z, $C_f = 0.1375(z_{rgh}/H)^{1/4}$ is the friction coefficient, and z_{rgh} is the roughness coefficient.

The initial conditions written in cylindrical coordinate system (r,z,φ) have the form:

$$\begin{aligned}
U_j &= U_0\, f_r(r/R_0)\, f_z(z)\sigma(R_0 - r),\\
\omega_z &= \omega_0\, f_r(r/R_1)\, f_z(z)\omega(R_1 - r),\\
J &= (J_0 - J_{bk})\,(1 - r^2/R_1^2)\, f_z(z)\sigma(R_1 - r),\\
U_r &= U_z = \omega_r = \omega_\varphi = a = 0,
\end{aligned} \tag{10}$$

where $f_r(\xi) = 4\xi(1 - \xi)$, $f_z(z) = \ln(1 + z/z_{rgh})/\ \ln(1 + H/z_{rgh})$, $R_1 = R_1(z) = J_{bk}^{1/2} + (0.5R_0 - J_{bk}^{1/2})\cdot(2z/H)\ e^{1 - 2z/H}$, R_0 is the size of the initial mesovortex cloud, U_0, ω_0, J_0 are the initial magnitudes, and $\sigma(r)$ is the Heaviside function.

We have solved the initial boundary problem (8)-(10) numerically with the modified Runge – Kutta – Adams –"leapfrog" scheme (MRKAL) [15-16]. The MRKAL scheme is conditionally stable and has the second order of accuracy in time and space. Its stability criterion is close to that of the evident McCormack scheme [33]. In brief, the algorithm can be written as follows. Let $\boldsymbol{y}^{(n)}{}_\Xi = \{a, J, \boldsymbol{U}, \boldsymbol{F}\}^{(n)}{}_\Xi$ and $\boldsymbol{u}^{(n)}{}_\Xi = \{J, \boldsymbol{U}, \boldsymbol{F}\}^{(n)}{}_\Xi$ refer to the mesh point Ξ at the time layer $t_n = n\tau$, where τ is the integration time-step (index Ξ is later omitted). Assuming that all the values are known at the n-th and $(n-1)$-th layers, we get the values at the sub-layer $(n+1/4)$ with the simple Adams' interpolation: $\boldsymbol{y}^{(n+1/4)} = 1.25\ \boldsymbol{y}^{(n)} - 0.25\ \boldsymbol{y}^{(n-1)}$. Then the $(n+1)$-th time layer is calculated as follow:

$$\begin{aligned}
u^{(n+1/2)} &= u^{(n)} + 0.5\tau\Pi_u[y^{(n+1/4)}],\\
a^{*(n)} &= 0.5\,(a^{(n-1)} + a^{(n)}) + 0.5\tau\Pi_a[y^{(n)}],\\
a^{(n+1/2)} &= a^{*(n)} + 0.5\tau\Pi_a[y^{(n)}],\\
u^{(n+1)} &= u^{(n)} + \tau\Pi_u[y^{(n+1/2)}],\\
a^{(n+1)} &= a^{*(n)} + \tau\Pi_a[y^{(n+1/2)}],
\end{aligned}$$

where $\Pi_a[\ldots]$ and $\boldsymbol{\Pi}_u[\ldots]$ are the right parts of (8) written in finite-differences. More details on the numerical algorithm can be found in [15-16].

The calculations were performed on two clusters: the ISP RAS cluster (AMD AThlon XP 1500 + Myrinet and Dual-Coré Intel® Xeon® 5160 Myrinet 2000) and cluster MVS1000M JSCC RAS (processors Power 2.2 GHz, Myrinet, 2 Gbit/s). Program implementation in different cluster architectures without code changes became possible due to portability features of the Parjava program environment [34]. Multi sequencing was performed by 2D division of the computational area, which strongly decreased the amount of data transfer. The optimization of parallel calculations, depending on partition method, matrix scale and processor number, was discussed in [15, 16].

5. RESULTS OF 3D TORNADO NUMERICAL MODELING

The initial boundary problem (8)-(10) has been solved with the initial data relevant to a mid-size T3 category tornado in the cubic area: $2L_1=H=1500$ m. The radius of initial mesovortex cloud $R_0=300$ m, initial cyclonic wind is calm with its magnitude: $U_0=1.5$ m/s, total kinematic viscosity coefficient $A=1000$ m^2s^{-1}, and

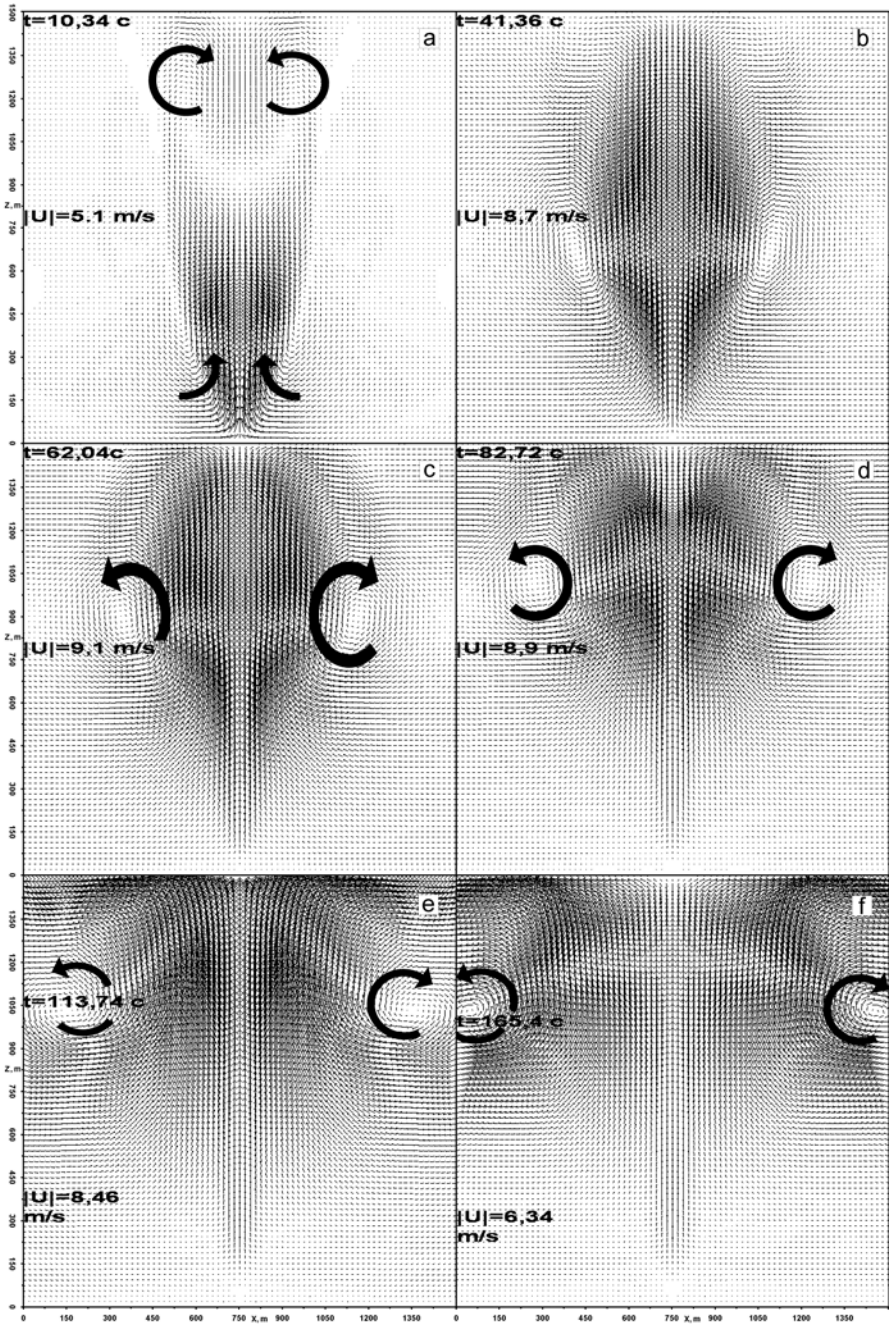

Figure 3: The winds in the central vertical cross-sections of the model tornado at different instants.

the roughness z_{rgh}=0.1 m. To describe the initial mesovortex activity, which is the main source of tornado rise in our model, the following dimensionless data is used: α_2 = 0.02, Π_M=0.5(1+ω_{rel})J_{rel}=750, Π_V=0.5α_2 (1+ω_{rel}) =120, where ω_{rel}=$\omega_0 R_0/U_0$=ω_0/Ω_0 and J_{rel}=J_0/R_0^2 are the relative mesovorticity and moment of inertia, correspondingly. It was shown [11,12] that the process of tornado (and hurricane) rise is mainly regulated by these three dimensionless parameters. The rest two parameters are as follows: J_{bk}=0.05J_0 and ω_{bk}=0.01ω_0. The number of mesh points in each direction is 80, and the time-step $\tau\cong$0.35 s.

The wind projections in the different cross-sections at the different instants are shown in Figures **3**, **5-7**. The coordinates in figures and in (8)-(10) are connected as follows: X=x+750 m, Y=y+750 m, Z=z (so, the central vertical axis of the tornado is at X=Y=750 m). Each vector field in each figure is normalized to unity. The absolute values of the radial-vertical winds shown in Figure **3** can be estimated by using Figure **4** and those of the horizontal ones shown in Figures **5**-**7** – by using Figure **8**.

The radial-vertical winds in the central cross-section, $\boldsymbol{U}_{xz}$={U_x,U_z}(X, 750 m, Z, t), are shown in Figure **3** at the following instants: a) 10.34 s, b) 41.36 s, c) 62.94 s, d) 82.72 s, e) 113.7 s, f) 165.4 s. The mean square velocity values $|U|\equiv\|\boldsymbol{U}(\boldsymbol{X},t_k)\|_{L2(D)}$ are also given in the figure.

Big black round arrows in Figure **3** are placed around the main instant centers of vertical – radial circulation. Note, that at t=0 both vertical and radial components are absent; only a slow cyclonic tangential motion exists with the amplitude of U_0=1.5 m/s.

The vertical–radial wind circulation is created due to interaction of the macroscale velocity (i.e. the observed winds) with the mesoscale vortices. The main instant centers of vertical-radial circulation ascend and move away from the center axis with time. The initial energy of mesovortices is transferred to the winds energy; the wind velocity grows up fast, until it reaches its maximal magnitude, and then slowly decays, what is typical to tornados and hurricanes.

The macroscale air circulation can be described as the suction of the surface air from the periphery towards the tornado center. Then, inside the eyewall, the air masses ascend till about 1 km height where they diverge to the periphery and descend. In this way, the tornado structure is creating.

The maximal vertical wind velocity U_z=31 m/s is reached in the center at $Z\approx$600 m and t = 51.7 s. At that instant, the maximal radial inflow $U_r \cong -7$ m/s and outflow $U_r \cong$ 5 m/s are located, respectively, at Z=500 m, r=230 m and Z=1200 m, r=330 m. Under the given parameters, the total typical mushroom-like structure of

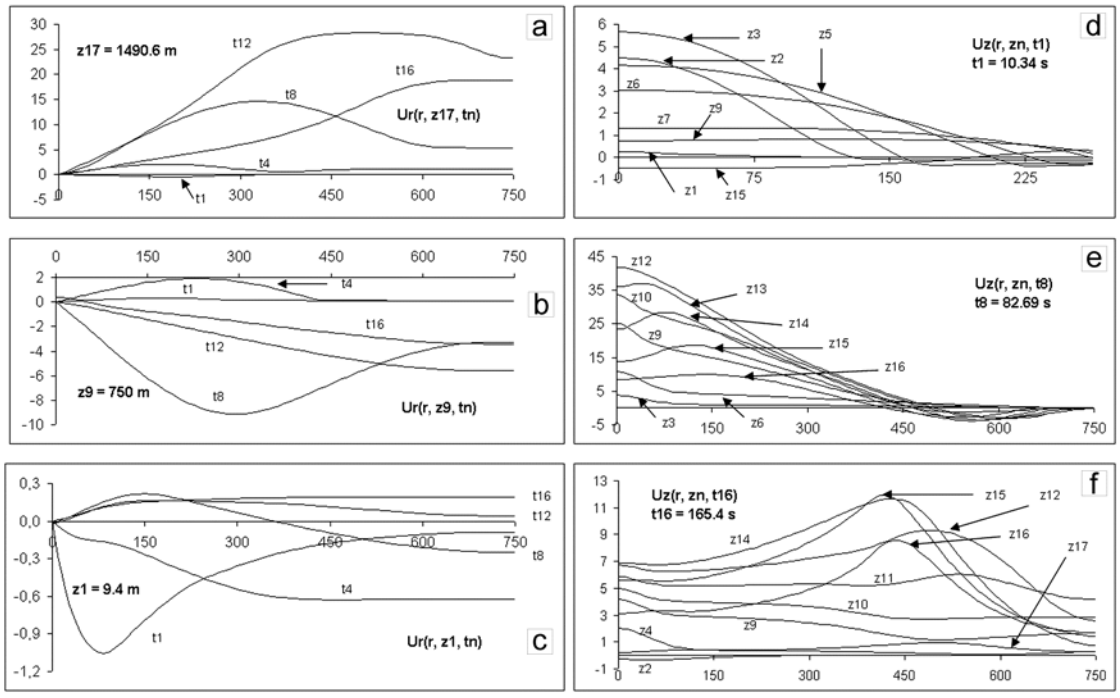

Figure 4: The radial U_r(r,zn,tn) (**a-c**) and vertical U_z(r,zn,tn) (**d-f**) winds (m/s) as functions of radius (φ=0) at the heights (m): z=zn=93.75·(n-1), n=2,...,16, z1=9.4, z17=1490, and the instants (s): t=tn=10.34·n.

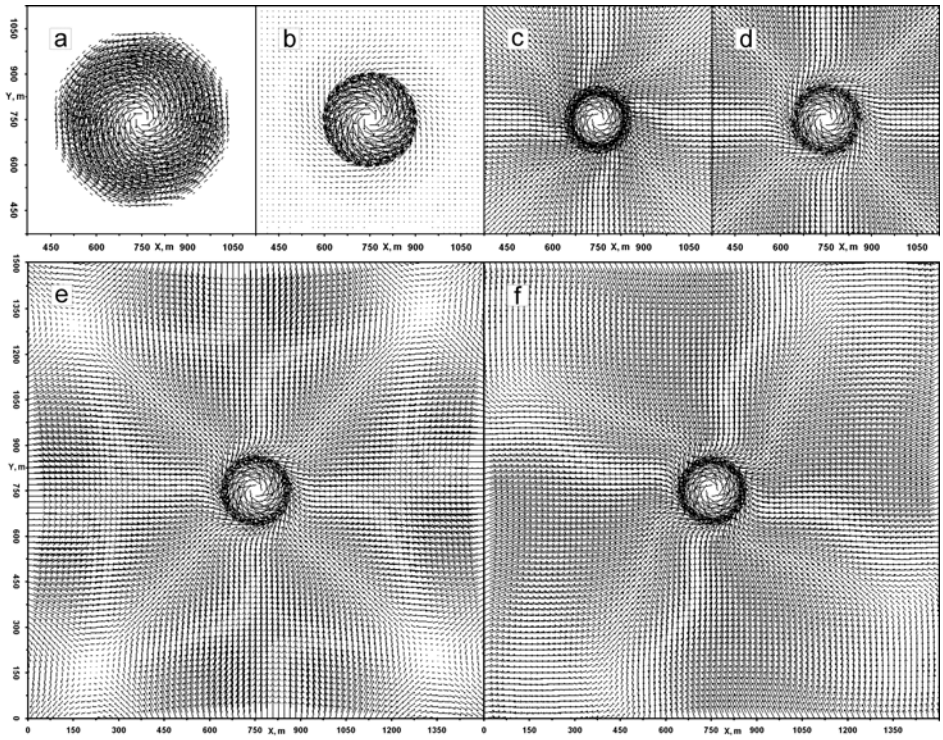

Figure 5: Horizontal winds at the height z=187.5 m at the instants (s): **a**) 0; **b**) 10.34; **c**) 41.36; **d**) 82.72; **e**) 124.1; **f**) 165.4.

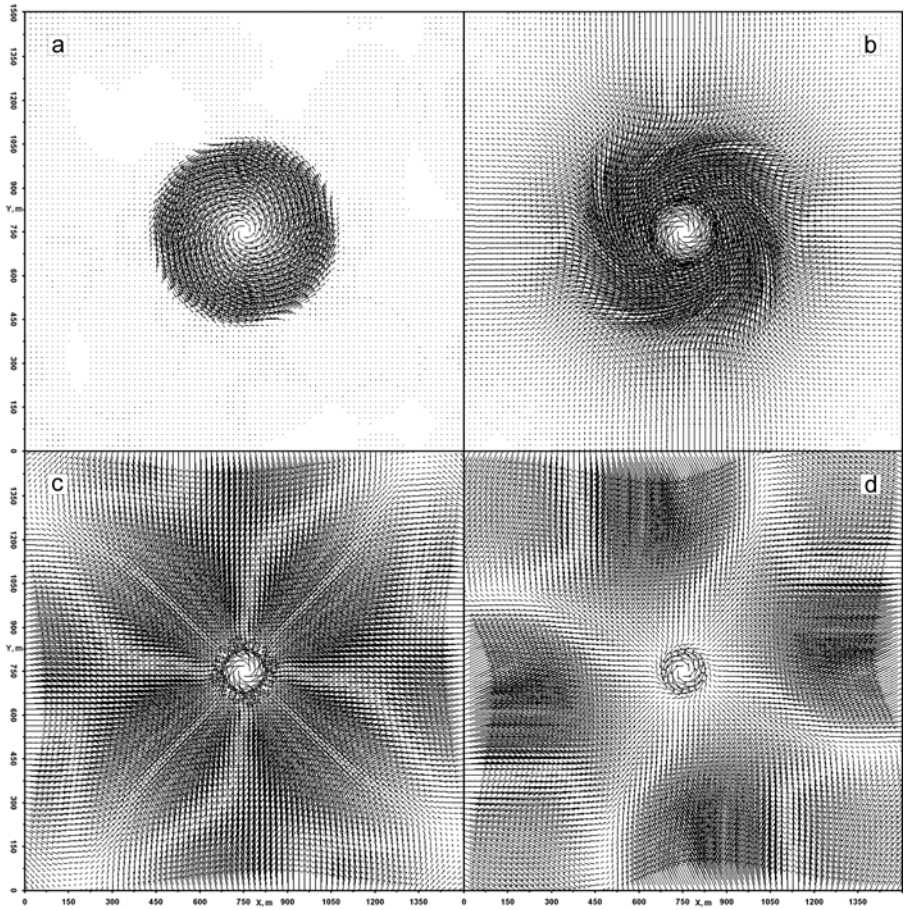

Figure 6: Horizontal winds at the height z=750 m at the instants (s): **a**) 20.7; **b**) 72.4; **c**) 103.4; **d**) 165.4.

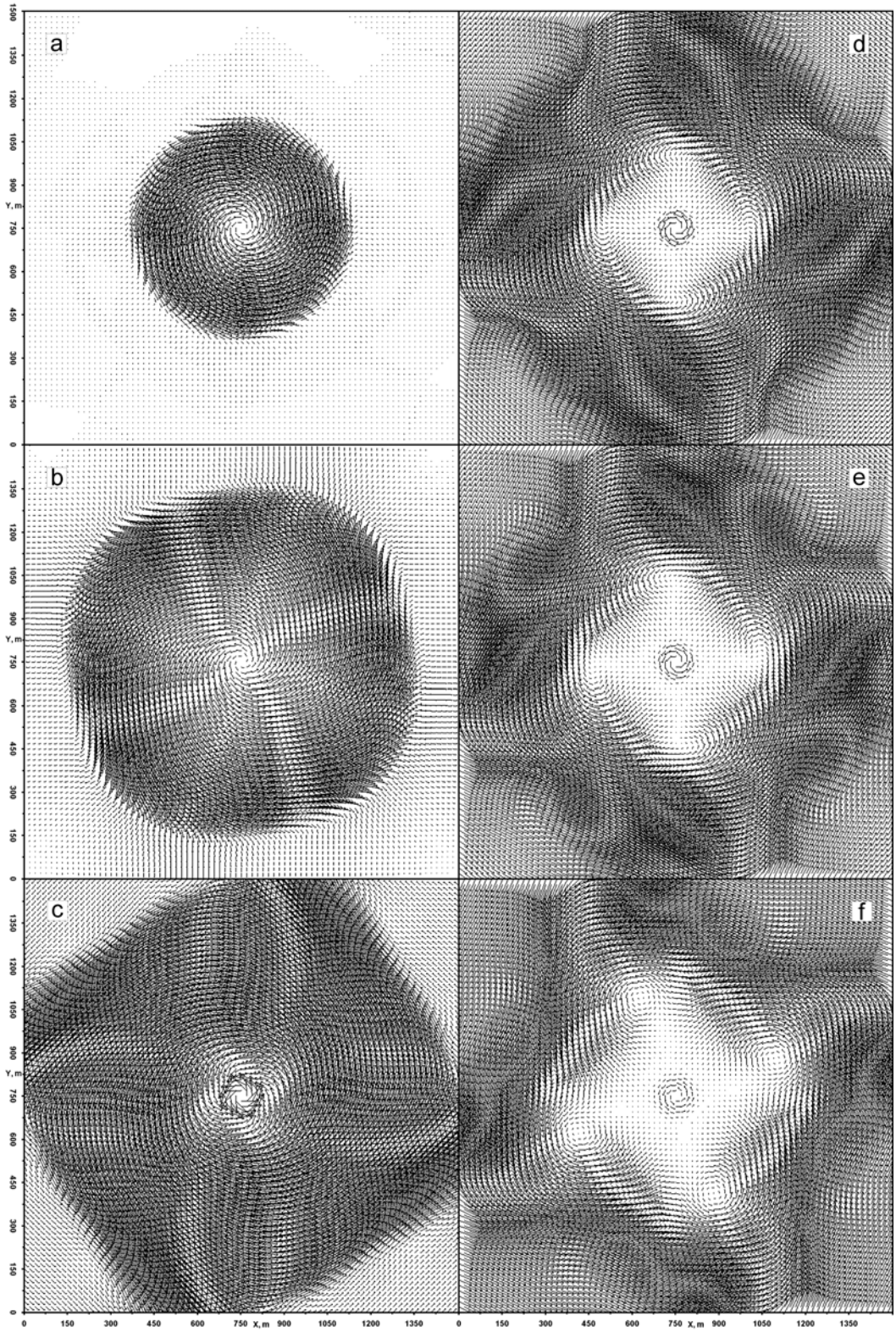

Figure 7: Horizontal winds at the height z=1125 m at the instants (s): **a**) 31; **b**) 72.4; **c**) 103.4; **d**) 134.4; **e**) 144.8; **f**) 165.4.

the tornado is formed approximately for a minute (Figures **3c**-**f**).

Figure **4** shows the radial $U_r(r,zn,tn)$ (a-c) and vertical $U_z(r,zn,tn)$ (d-f) winds (in m/s) at the heights (in meters): $z=zn=93.75\cdot(n-1)$, $n=2,...,16$, $z1=9.4$, $z17=1490$, and the time instants (in seconds): $t=tn=10.34\cdot n$, as the functions of radius at the azimuth angle $\varphi=0$ ($y=0$, $x>0$).

The horizontal winds $\boldsymbol{U}_{xy}=\{U_x,U_y\}(X, Y, Z, t)$ at the different instants and heights are shown in Figures **5**-**7**:

Figure **5**: Z=187.5 m; a) 0 s, b) 10.34 s, c) 41.36 s, d) 82.72 s, e) 124.1 s, f) 165.4 s;

Figure **6**: Z=750 m; a) 20.7 s, b) 72.4 s, c) 103.4 s, d) 165.4 s;

Figure **7**: Z= 1125 m; a) 31 s, b) 72.4 s, c) 103.4 s, d) 134.4 s, e) 144.8 s, f) 165.4 s.

Figure **8** shows the horizontal wind amplitudes $U_{hor}(z,t)= \max|\boldsymbol{U}_{xy}|(|x|,|y|<L_1)$ at four heights.

At t=0 s and all the heights, there are no radial (and vertical) winds, and the current represents pure tangential rotation inside the radius $r\le R_0$=300 m. The initial structure of the horizontal winds at all the heights is like the one shown in Figure **5a** (Z=187.5 m), and only tangential velocity magnitude varies with height.

E.g. at Z=187.5 m the initial azimuth wind velocity magnitude equals to 1.2 m/s. With time at that height, the radial flux towards the eyewall arises and grows. During the first *10 seconds* the horizontal velocity increases in *10 times* and reaches 12 m s^{-1}, while the eyewall radius narrows to $r\le$153 m (Figure **5b**). Later on, the eyewall radius still decreases tending to be stabilized near $r\approx$110 m (Figures **5c**-**f**).

Both inside and out of the eyewall, the air cyclonically spirals towards the wall. But out of the eyewall the air motion reveals more complicated features with time. For example, at the corners of Figure **5e** (t=124.1 s) one can clearly see conglomerates of four vortices of different polarity, where the horizontal flow recalls a jet normally striking a bar.

The magnitude of horizontal wind at this height reaches its maximum of about 14 m/s in 12 seconds and afterwards begins to decrease, while the gradient of the vertical velocity is still growing (compare with Figures **3d-f**).

At Z=750 m (Figure **6**) the evolution of the horizontal winds resembles that at z=187.5 m (Figure **5**) with the only difference that the maximum of horizontal wind velocity is greater (about 28 m/s) and is reached later (in about 22 sec). One can clearly see the growth of the eyewall thickness (Figure **6b**), and more intense and complicated motions at the periphery (Figures **6c-d**).

At the height Z=1125 m (Figure **7**) the maximum of the horizontal velocity is about 30 m/s and is reached approximately in 31 seconds (Figures **7a** and **8**). At this height and higher, the centrifugal trend appears – the air outflow towards the periphery, growing in time (Figures **7b-e**; see also Figures **3c-f** and **4a**). The eyewall expands and occupies the area up to r = 550 m at t = 72.4 s (Figure **7b**) and after t=103.4 s intense horizontal currents cover the whole calculation area (Figures **7c-f**).

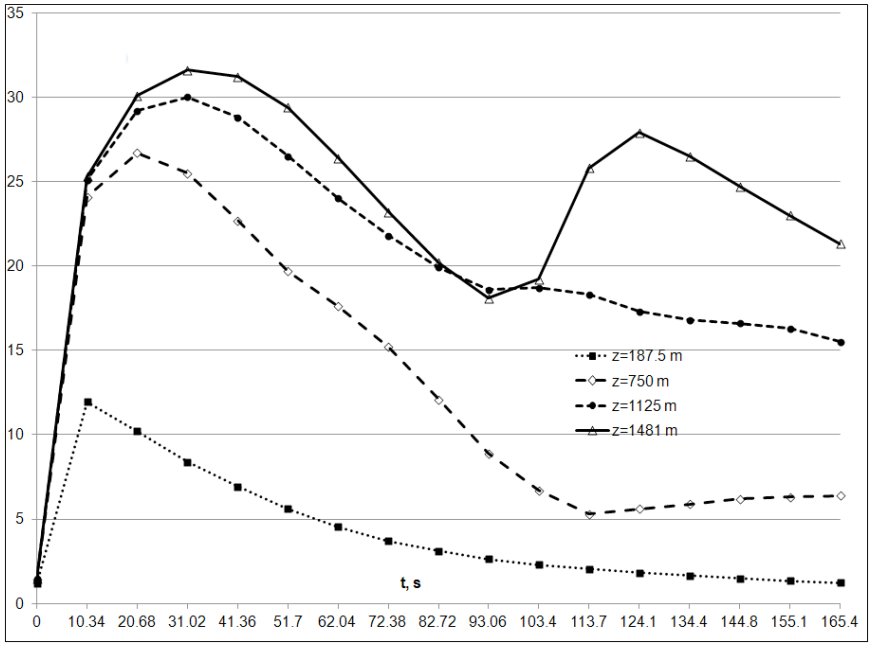

Figure 8: The magnitudes of horizontal winds $U_{hor}(z,t)$ (m/s) with time (seconds) at the different heights z.

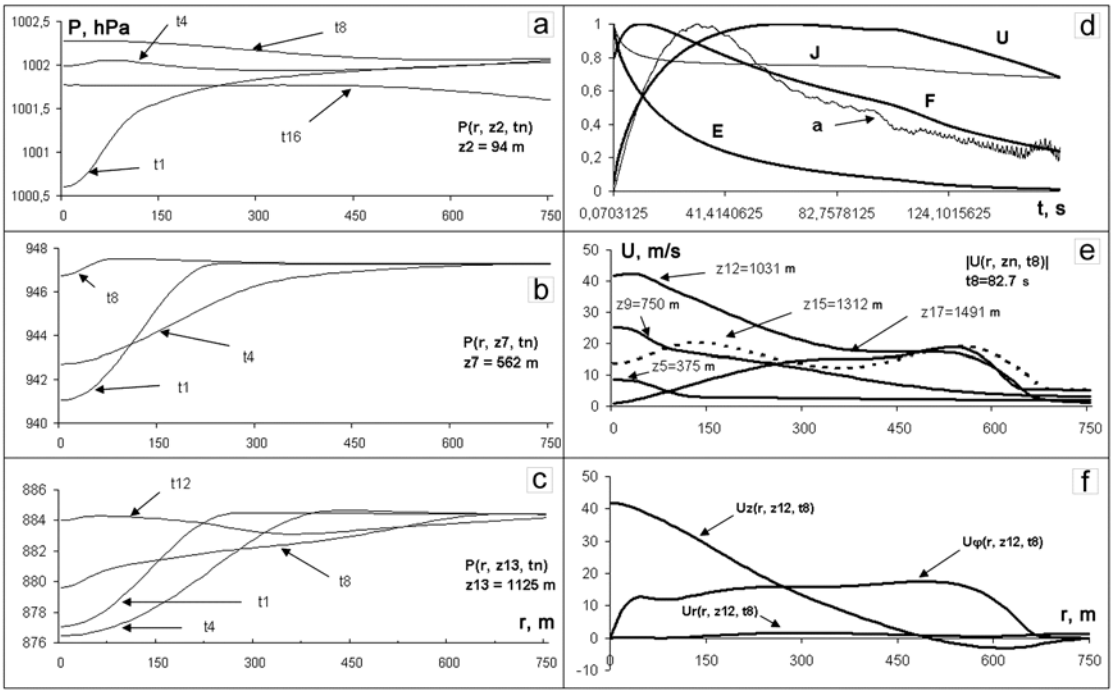

Figure 9: (**a-c**): pressures at the different heights and instants; (**e**): wind velocity magnitudes at the instant when absolute maximum wind is reached at t=82.7 s; (**f**): wind components (t=82.7 s, z=1031.25 m) (**d**): the total energy E, wind U, moment of mass J, total vorticity F, and the dencity parameter a, unity-normalized in square norms. The time instants and heights are the same as in Figure **4**.

After t>100 s the secondary vortices emerge at the inner edge of the eyewall at r≈260 m (Figure **7d**). The system of four secondary vortices is relatively stable and cyclonically turns (counterclockwise) with angular velocity ω_{SV}≈0.0116 s^{-1} (Figures **7d-f**).

Such subtornado-scale multiple vortices structures have been observed visually or in patterns of havoc [17-20], by numerical [21] and laboratory [22] simulations, and by Doppler Radars [23]. Similar patterns of the eyewall mesovortices rotating around the eye center, emerging, coupling, decaying, and again merging, are also observed in severe hurricanes [24-26].

To estimate the quantitative values of the horizontal winds shown in Figures **5-7** one can use Figure **8**: the maximal arrow length in each of these figures corresponds to the respective value of $U_{hor}(z,t)$ in Figure **8**.

Figure **9** shows the main dynamic features of the numerical model. The central depression forming in the center of the category T3 tornado is shown in Figures **9a-c**. The typical pressure pit shown in these figures, as well as the wind velocity radial distributions at different heights at the instant of maximal winds shown in Figures **9e-f**, sufficiently good correspond to the observation data [11,12,14]. The unity-normalized mean square values of the total energy (E), wind velocity (U), moment of mass (J), total vorticity (F), and the density parameter (a) as the functions of time are shown in Figure **9d**. The time instants (t_k) and heights (z_n) are the same as described in Figure **4**.

6. DISCUSSION

Figure **10** shows visual comparison of our numerical model (in quasi-3D form) with the photograph of the category T3 tornado made in Montana, USA, August 2005.

The structure of the objects in either picture is practically the same. Moreover, the space, time and the velocity data in our numerical experiment and the observed tornado almost coincide.

Another visual comparison is shown in Figure **11** where the model tornado at the instant t=93 sec is compared with the 1973 Union City, Oklahoma tornado. It was the first tornado captured by the National Severe Storms Laboratory Doppler radar, and it is shown here in its early stage of formation[4].

[4]http://celebrating200years.noaa.gov/breakthroughs/tornadowarnings/01_tornado650.html

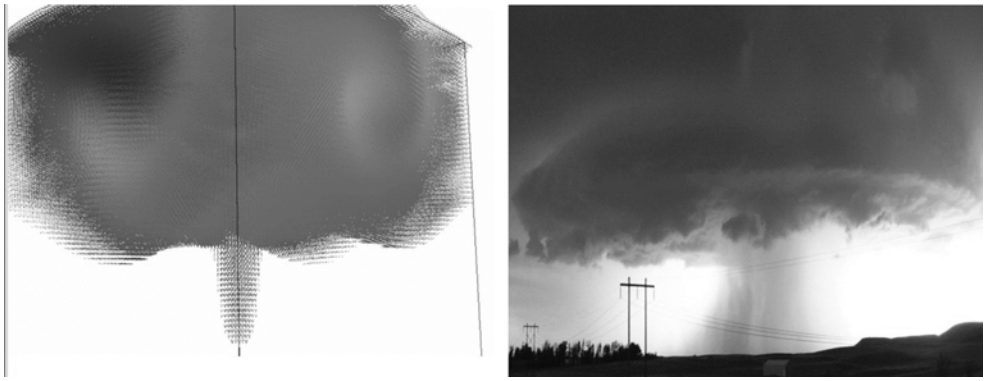

Figure 10: Left: 3D wind field in our model at t=165.4 s. Right: snapshot of T3 tornado, Montana, USA, August 2005 (Andrei Panshin © 2005).

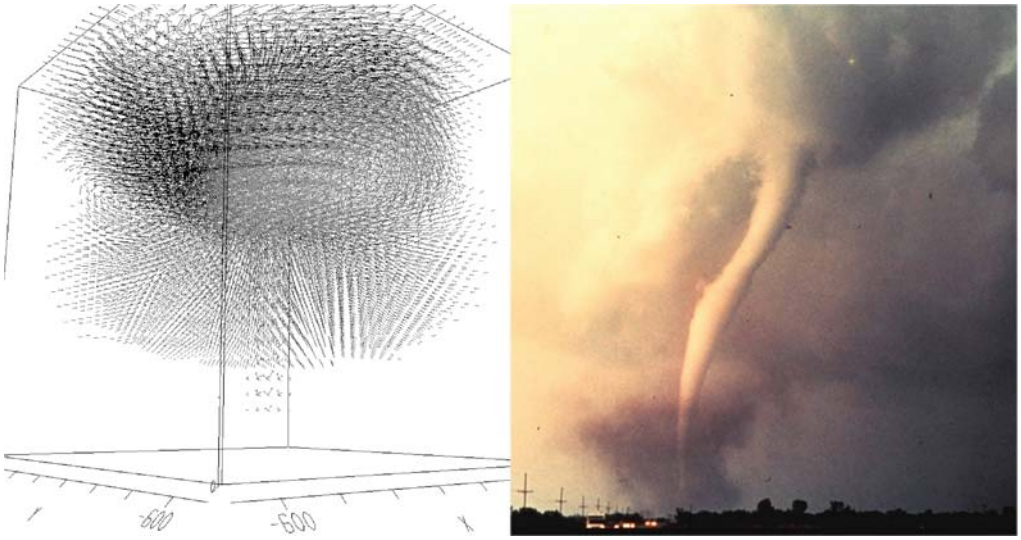

Figure 11: Left: 3D wind field in our model at t=90.03 s. Right: 1973 Union City, Oklahoma tornado in it early stage of formation.

Concerning multiple vortices formation shown in Figure **7d-f**, it is interesting to compare it with the similar phenomena observed in violent hurricanes.

Figure **12** shows the satellite GOES-12 photograph of Hurricane Isabel, September 13, 2003, 1812 UTC (left) and the horizontal cross-section of the model tornado at t=165.4 s, z=1125 m (right). The both reveal four "pin-wheel" vortices around the central one. We found the following estimates for the diameters of eyewalls: D_e=70 km (Isabel), d_e =1.1 km (our model); central vortices: D_c=24.6 km, d_c=0.37 km; "pin-wheel" vortices D_p=19.4 km, d_p=0.27 km; and the radii of the "wheels": R_w=25 km, r_w=0.36 km. The geometrical similarity of the vortices in the eye of Hurricane Isabel and those of the tornado calculated in our model is obvious.

Another comparison of the model tornado and Hurricane Isabel can be made by rescaling in time, space, and velocity. Concerning the maximal wind velocity (MWV) in our model $U_{MW}(t)=\|\boldsymbol{U}(\boldsymbol{X},t)\|_{C(D)}$ and the best-track wind velocity (BTV) in Hurricane Isabel $U_{BT}(t)$ [25], we can normalize MWV to BTV: $U_{MWN}(t)=k_U U_{MW}(t)$, where k_U is the relation of absolute maximum of BTV (74.9 m/s) to that of MWV (42.11 m/s). Then, let us define the typical time scale of Hurricane Isabel T_I as the time period since 0000 UTC 6 September 2003, when it became a tropical depression from an African easterly wave with BTV=16.4 m/s, until 1200 UTC 11 September 2003, when it reached the peak BTV. In the same manner we define the typical time scale of the model T_M as the time period while the normalized MWV is rising from 16.4 m/s to its peak value 74.9 m/s. Rescaling the model time rate with the factor $k_T=T_I/T_M \cong 5233$, we then can compare the time-rescaled normalized MWV $U_{MWNT}(t)= U_{MWN}(t/k_T)$ of the model with the BTV of Hurricane Isabel. The results of the comparison are shown in Figure **13**.

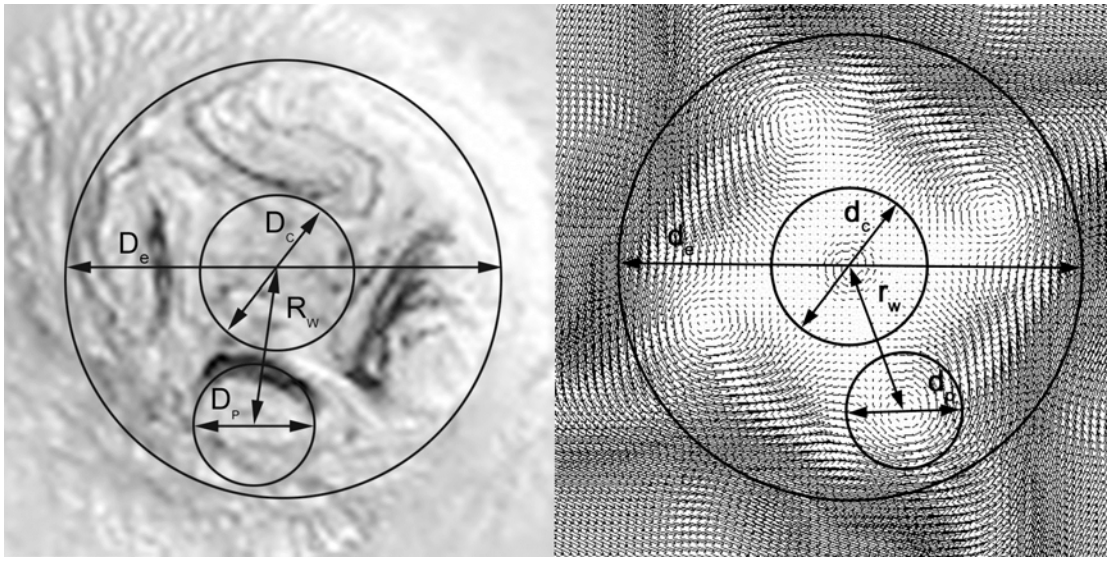

Figure 12: Left: the eye of Hurricane Isabel (zoomed part of GOES-12 photo, Sept. 13, 2003, 1812 UTC, http://goes.gsfc.nasa.gov/pub/goes/030913.isabel.gif). Right: the eye of the model tornado at t=165.4 s, z=1125 m. (See details in text).

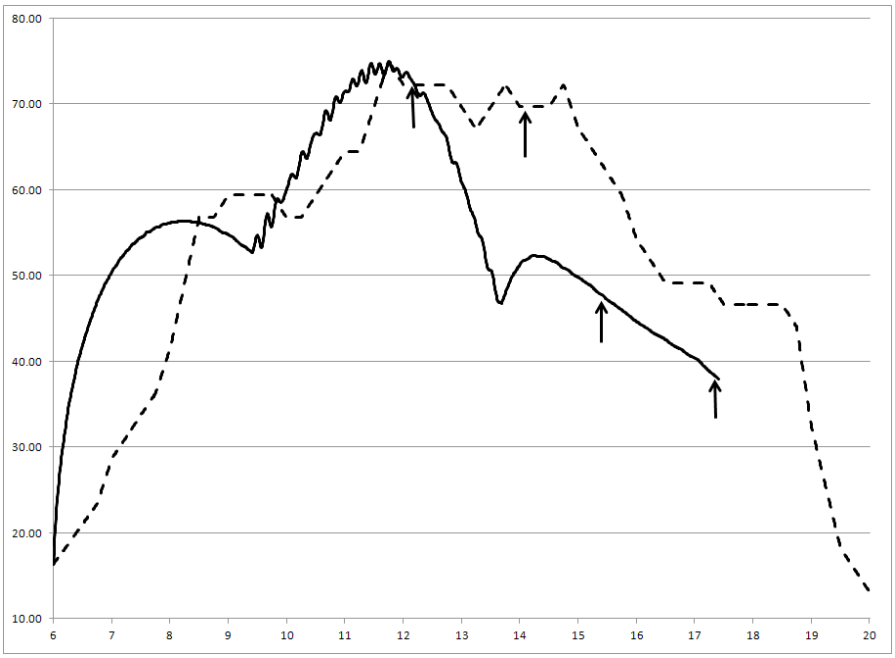

Figure 13: Best-track wind velocity (m/s) in Hurricane Isabel [*25*] (dashed) and rescaled maximal wind velocity in the model (solid). Horizontal axis shows time in days of September 2003. The arrows show the periods when multi-vortices inside the hurricane/tornado model were observed/ calculated.

The spatial coordinates of the model should be rescaled by the factor $k_X=D_e/d_e\cong 63.63$, and the similarity law requires $A_I=A_M\, k_X^2/k_T$, where A_I and A_M are the typical turbulent viscosity coefficients of the hurricane and the model, respectively. In the numerical model A_M =1000 m^2s^{-1}, so the effective turbulent viscosity in the hurricane should be equal to $A_I \cong 774$ m^2s^{-1}, what is in good agreement with the observation data.

7. CONCLUSION

The Cosserat model of asymmetrical hydrodynamics is applied to the tornado/hurricane phenomena which differ in their scales and nature. The tornado rise from the cloud of turbulent eddies is considered as the localization process. Our numerical solution of the problem applied to Category 3 tornado proved its fitness.

Our model concept is to overcome the prejudice against the vortex symmetry of turbulence microstructure, and the alternative concept of gradient homogeneity is suggested which agrees with the Kolmogorov idea of local isotropy.

Interesting features of the concept implemented here are as follows. First, our model can explain multiple vortices formation both in tornados and hurricanes simultaneously (depending on the scale factors), and, second, it is shown that the mesoscale theory of turbulence can explain the processes of catastrophically rapid rise of tornados (or hurricanes), and also can describe the peculiar features of these phenomena, such as multiple vortices.

REFERENCES

[1] Selected Works of A.N. Kolmogorov: Volume I: Mathematics and Mechanics. V.M. Tikhomirov, Ed., Kluwer, Dordrecht, 1991.

[2] Taylor G.I. Statistical Theory of Turbulence. Proc R Soc London Ser A 1935; 151: 421-478. http://dx.doi.org/10.1098/rspa.1935.0158

[3] Schrodinger E. What is life? Cambridge Univ. Press, 1944.

[4] Cosserat E. et F. Theorie des Corps Deformables. Herman, Paris, 1909.

[5] Nikolaevskiy V.N. Angular Momentum in Geophysical Turbulence: Continuum Spatial Averaging Method. Kluwer, Dordrecht 2003. http://dx.doi.org/10.1007/978-94-017-0199-0

[6] Nikolaevskiy V.N. Asymmetrical Mechanics of Continua and Averaged Description of Turbulent Flows. Dokl Akad Nauk 1969; 184(6) 1304-1307 [in Russian].

[7] Mattioli G.D. Teoria Dinamica dei Regimi Fluidi Turbolenti. CEDAM, Pardova 1937.

[8] Ferrari C. On the Differential Equations of Turbulent Flow. In: Continuum Mechanics and Related Problems of Analysis, Nauka, Moscow 1972; pp. 555-566.

[9] Heinloo J. Setup of turbulence mechanics accounting for a preferred orientation of eddy rotation // Concepts of Physics 2008; 5: 205-219. http://dx.doi.org/10.2478/v10005-007-0033-8

[10] Eringen A.C., Chang T.S. A Micropolar Description of Hydrodynamic Turbulence. In: Recent Advances in Engineering Science, Gordon & Breach, New York 1970; 5(2): 1-8.

[11] Arsenyev S.A., Gubar A.Yu., Nikolaevskiy V.N. Self-Organization of Tornados and Hurricanes in Atmospheric Currents with Meso-Scale Eddies. Dokl Earth Sci 2004; 396(4): 588-593. [Doklady Akademii Nauk 2004; 396(4): 541-546].

[12] Arsenyev S.A., Babkin V.A., Gubar A.Yu., Nikolaevskiy V.N. Theory of Mesoscale Turbulence. Eddies of the Atmosphere and the Ocean. RCD, Moscow – Izhevsk, 2010. [in Russian].

[13] Arsen'ev S.A., Gubar A.Yu., Shelkovnikov V.N. Generation of Typhoons and Hurricanes by a Mesoscale Turbulence. Moscow Univ Phys Bull 2007; 62(2): 113-117. [Vestnik Moskovskogo Universiteta Fizika 2007; 62(2): 50-54]. http://dx.doi.org/10.3103/S0027134907020129

[14] Gubar A.Yu., Avetisyan A.I., Babkova V.V. Tornado Rise: 3D Numerical Model in Mesoscale Turbulence Theory of Nikolaevskiy. Dokl Earth Sci 2008; 419(2): 467-472. [Doklady Akademii Nauk 2004; 419(4): 547-552]. http://dx.doi.org/10.1134/S1028334X08030264

[15] Avetisyan A.I., Babkova V.V., Gaissaryan S.S., Gubar' A.Yu. Development of Parallel Software for Resolving the 3D Task about the Origin of the Tornado According to the Nikolaevskii Theory. Math Models Comput Simul 2009; 1(4): 482-492 [Matematicheskoe Modelirovanie 2008; 20(8): 28-40]. http://dx.doi.org/10.1134/S2070048209040061

[16] Avetisyan A.I., Babkova V.V., Gaissaryan S.S., Gubar A.Yu. Intensive Atmospheric Vortices Modeling Using High Performance Cluster Systems. LNCS 2007; 4671: 487-495. doi:10.1007/978-3-540-73940-1_48

[17] Fujita T.T. The Lubbock tornadoes: A Study of Suction Spots. Weatherwise 1970; 23(4): 161-173. http://dx.doi.org/10.1080/00431672.1970.9932888

[18] Agee E.M., Church C., Morris C., Snow J. Some synoptic aspects and dynamic features of vortices associated with the tornado outbreak of 3 April 1974. Mon Wea Rev 1975; 103: 318-333. http://dx.doi.org/10.1175/1520-0493(1975)103<0318:SSAADF>2.0.CO;2

[19] Agee E.M., Snow J.T., Nickerson F.S., Clare P.R., Church C.R., Schaal L.A. An Observational Study of the West Lafayette, Indiana, Tornado of 20 March 1976. Mon Wea Rev 1977; 105: 893-907. http://dx.doi.org/10.1175/1520-0493(1977)105<0893:AOSOTW>2.0.CO;2

[20] Pauley R.L., Snow J.T. On the Kinematics and Dynamics of the 18 July 1986 Minneapolis Tornado. Mon Wea Rev 1988; 116: 2731-2736. http://dx.doi.org/10.1175/1520-0493(1988)116<2731:OTKADO>2.0.CO;2

[21] Rotunno R. Numerical Simulation of a Laboratory Vortex. J Atmos Sci 1977; 34: 1942-1956. http://dx.doi.org/10.1175/1520-0469(1977)034<1942:NSOALV>2.0.CO;2

[22] Church C.R., Snow J.T. Laboratory Models of Tornadoes. In: Church C., Burgess D., Doswell C., Davies-Jone R., Eds., The Tornado: Its Structure, Dynamics, Prediction, and Hazards, Am. Geophys. Union, Washington, D.C., 1993; pp. 19-39. doi:10.1029/GM079p0277

[23] Wurman J. The Multiple-Vortex Structure of a Tornado. Wea. Forecasting 2002; 17: 473-505. http://dx.doi.org/10.1175/1520-0434(2002)017<0473:TMVSOA>2.0.CO;2

[24] Montgomery M.T., Vladimirov V.A., Denisenko P.V. An Experimental Study on Hurricane Mesovortices. J Fluid Mech 2002; 471: 1-32. http://dx.doi.org/10.1017/S0022112002001647

[25] Bell M.M. & Montgomery M.T. Observed Structure, Evolution, and Potential Intensity of Category 5 Hurricane Isabel (2003) from 12 to 14 September. Mon Wea Rev 2008; 136: 2023-2046. http://dx.doi.org/10.1175/2007MWR1858.1

[26] Kossin J.P., Schubert W.H. Mesovortices in Hurricane Isabel. Bull Am Meteorol Soc 2004; 85: 151-153. http://dx.doi.org/10.1175/BAMS-85-2-151

[27] Poincare H. Theorie des Tourbillions. Carré et Naud, Paris. 1893.

[28] Batchelor G.K. An introduction to fluid dynamics, Cambridge University Press, 1967, 1973, 2000, First Cambridge Mathematical Library edition 2000 Reprinted 2001, 2002. XVIII, 615 p. — ISBN 0 521 66396 2 (paperback).

[29] Brode H.L. Review of Nuclear Weapon Effects. Annu Rev Nucl Sci 1968; 18: 153-202. http://dx.doi.org/10.1146/annurev.ns.18.120168.001101

[30] Obukhov A.M. Turbulence for Atmospheric Dynamics. Center for Turb. Res., Palo Alto, Calif., 2001.

[31] Iovieno M., Tordella D. The Angular Momentum Equation for a Finite Element of a Fluid: A New Representation and Application to Turbulent Modeling. Phys Fluids 2002; 14(8): 2673-2682. http://dx.doi.org/10.1063/1.1485765

[32] Iskenderov D.Sh, Nikolaevskiy V.N. Laminar Core of Atmospheric Turbulent Eddies. Dokl Akad Nauk 1991; 319(1): 124-128. [in Russian].

[33] Fletcher C.A.J. Computational Techniques for Fluid Dynamics. Vol. II: Specific Techniques for Different Flow Categories. Springer-Verlag, Berlin 1988.

[34] Ivannikov V.P., Gaissaryan S.S., Avetisyan A.I., Padaryan V. A. Improving Properties of a Parallel Program in ParJava Environment, LNCS 2003; 2840: 491–494. http://dx.doi.org/10.1007/978-3-540-39924-7_65

Received on 30-05-2014 Accepted on 06-07-2014 Published on 30-09-2014

DOI: http://dx.doi.org/10.15377/2409-5710.2014.01.01.1